Title

Zero-padded fast Fourier transform reveals new dominant frequency pattern in optical maps during ventricular fibrillation

Authors
Peng-Wie Hsia, PhD
Suresh E Joel, M.Sc.

Affiliation
Department of Biomedical Engineering, Virginia Commonwealth University

Support in part by a Whitaker Biomedical Engineering grant from Whitaker Foundation and by a Grant-in-Aid grant from Mid-Atlantic Consortium of American Heart Association

Corresponding Author
Peng-Wie Hsia, Ph.D.
Associate Professor, Department of Biomedical Engineering
1112 E Clay Street, PO Box 980694
Richmond VA 23298-0694 USA
Tel: 804-828-4976
Fax: 804-828-5459
Email: phsia@vcu.edu

Abstract

Fast Fourier transform (FFT) has been widely used to study fibrillation in optical maps by extraction of dominant frequency (DF) to represent rate of excitation in the cardiac tissue during fibrillation. Though *N*-point FFT (*N*-FFT) has served very well for frequency analysis of fibrillation waveforms, in this article we present different results using zero-padded FFT, a simple, well-established digital signal processing technique. In particular, certain nuances in DF maps could be observed only when ZP-FFT was used.

With simulated single harmonic waves and cardiac action potential waveforms, we show that DF detection is more accurate using ZP-FFT. In addition, for a set of randomly selected points from optical maps in isolated rabbit hearts, mean rate of excitation is shown to be better correlated to DF obtained by ZP-FFT than by *N*-FFT. In DF maps small changes in DF passed unnoticed when *N*-FFT was used. We observed for the first time that these small DF changes formed continuous DF gradients in area between two DF domains when ZP-FFT was used. The existence of smooth gradient distribution of DF values is a new finding. The characteristics of gradient DF are being studied in the context of its implication on epicardial VF propagation.

Introduction

Fast Fourier transform (FFT) algorithm has been extensively applied in many medical research fields including cardiac electrophysiology. Since 1990, a large number of publications (1576 publications) listing FFT as one of its keywords or abstract contents are reported in a recent literature search in PubMed (PubMed®, the National Library of Medicine's journal literature search system). In ventricular fibrillation (VF) studies, the FFT method has been recently used elegantly for examining the mechanism of fibrillation (Berenfeld et al. 2000;Berenfeld et al. 2002;Chen J et al. 2000;Mansour et al. 2001;Samie et al. 2001;Skanes et al. 1998;Valderrabano et al. 2002;Zaitsev et al. 2000).

Brief review of Fourier Transform Technique

Continuous Fourier transform: For an arbitrary discrete signal *x(n)* of *N* samples, the continuous Fourier transform (FT) can be expressed as below

$$X(\omega) = \sum_{n=0}^{N-1} x(n) e^{-j\omega n}, \quad -\pi \le \omega \le \pi \tag{1}$$

where $X(\omega)$ is the frequency spectra, function of a *continuous* variable, ω (Proakis & Manolakis 1996).

Discrete Fourier transform: For computer representation, $X(\omega)$ is sampled and digitized using discrete Fourier transform (DFT) formula. Commonly *N* equally spaced frequency samples are taken, called the *N*-point DFT (*N*-DFT) and is written as follows

$$X(k) = \sum_{n=0}^{N-1} x(n) e^{-j\frac{2\pi}{N}kn}, \quad k = 0,..., N-1 \tag{2}$$

where, *X(k)* are the sampled values of $X(\omega)$ at the following frequencies,

$$\omega = \frac{2\pi}{N} k, \quad k = 0,..., N-1 \tag{3}$$

Fast Fourier transform: FFT method is a computationally efficient algorithm for computing the DFT formula. For a signal of data length, *N*, traditional FFT method computes N-point FFT (*N*-FFT) to express *N*-DFT. The corresponding frequency resolution is 1/N (unit-less representation), i.e. the discrete frequencies are at 0, 1/N, 2/N, …, (N-1)/N. Since the frequency resolution is fixed and is inversely related to the data length (Oppenheim & Schafer 1975;Proakis & Manolakis 1996), the precision of frequency measurement is commonly assumed to be restricted by the frequency resolution.

Interpolating DFT: It is important to point out that Equations (2) and (3) are the sampled version of Equation (1). They contain the minimum required samples in the frequency domain to perform inverse DFT so *x(n)* can be reconstructed from the N samples in *X(k)*. $X(\omega)$ can also be reconstructed directly by sinc interpolation method using the N-samples in *X(k)* obtained using *N*-FFT. (Oppenheim & Schafer 1975;Proakis & Manolakis 1996):

$$X(\omega) = \sum_{k=0}^{N-1} X(k) p\left(\omega - \frac{2\pi}{N} k\right), \quad -\pi \le \omega \le \pi \tag{4}$$

where p(ω) is the interpolation kernel.

If more samples in the frequency spectrum are needed for any reason, it is possible to obtain by interpolating *X(k)*. However, it is computationally disadvantageous to realize Equation (4) directly. An equivalent but efficient method to obtain more frequency samples is to perform DFT on *zero-padded* signal, where the zero-padded data length *L>N.* This is commonly termed as zero-padded DFT (ZP-DFT). In both *N*-DFT and ZP-DFT, the FFT algorithm can be used resulting in *N*-FFT and the ZP-FFT.

Dominant frequency: Spectral peak detection has been widely used to extract dominant frequency (DF) in VF studies (Berenfeld, Mandapati, Dixit, Skanes, Chen, Mansour, & Jalife 2000;Berenfeld, Zaitsev, Mironov, Pertsov, & Jalife 2002;Chen J, Mandapatti R, Berenfeld O, Skanes A C, & Jalife J 2000;Mansour, Mandapati, Berenfeld, Chen, Samie, & Jalife 2001;Samie, Berenfeld, Anumonwo, Mironov, Udassi, Beaumont, Taffet, Pertsov, & Jalife 2001;Skanes, Mandapati, Berenfeld, Davidenko, & Jalife 1998;Valderrabano, Yang, Omichi, Kil, Lamp, Qu, Lin, Karagueuzian, Garfinkel, Chen, & Weiss 2002;Zaitsev, Berenfeld, Mironov, Jalife, & Pertsov 2000). Since the signal is nonstationary in such analyses, short data length is preferred which in turn reduces the frequency resolution. As is the case in many nonstationary signals, an unavoidable tradeoff between time localization and the frequency resolution exists. In this paper, we demonstrate that the *N*-FFT based frequency analysis could miss nuances in DF detection and could be erroneous. Although well-developed in the field of digital signal processing (Kay & Marple 1981), zero-padded FFT (ZP-FFT) has never

been applied in VF studies. We show that ZP-FFT having more frequency samples increases accuracy in DF detection.

We applied simultaneously both the *N*-FFT and the ZP-FFT methods to short data segments. The results using simple simulated signals as well as recorded optical mapping data during VF are presented. We observed that the degree of errors using traditional DF measurement could be small, in cases, only confined by frequency resolution while in others were large and could not be ignored. We show that the observed spatially discrete DF domains and uniform DF values within each domain reported previously (Samie, Berenfeld, Anumonwo, Mironov, Udassi, Beaumont, Taffet, Pertsov, & Jalife 2001;Zaitsev, Berenfeld, Mironov, Jalife, & Pertsov 2000), while using *N*-FFT, sometimes disappear when the DF values are measured with ZP-FFT. New spatial patterns of frequency gradient across DF domains were noticed only when DF was extracted using ZP-FFT. The impact to the understanding of the mechanism of VF is speculated.

Glossary of terms

DF - Dominant Frequency, frequency of the signal with maximum spectral power.

DF map – A map generated by extracting DF for each pixel in an optical map.

DFT – Discrete Fourier transform

FFT – Fast Fourier transform

HPDF map – High precision DF map obtained using ZP-FFT

N-FFT – N-point fast Fourier transform when the signal is of length N.

VF – Ventricular fibrillation

ZP-FFT – Zero-padded fast Fourier transform.

Methods and materials

Simulation studies

Simple single harmonic waves as well as action potential waveforms were simulated. DF was detected as the frequency with maximum power using two methods 1) *N*-FFT and 2) ZP-FFT. While using ZP-FFT, the signal was zero-padded to make data length 10*N*, so as to achieve 10 times the frequency samples as *N*-FFT. The accuracy of DF detection by the two methods was compared.

Simulated optical maps were constructed using single harmonic waves of specified frequency at each pixel. The pattern of frequency distribution was simulated to be similar to what was observed in experimental studies. DF maps were then extracted for these maps using both *N*-FFT and ZP-FFT. For more realistic simulation study, action potential waveforms of fixed cycle length were assigned to pixels to form DF patterns similar to that observed in experimental studies (these maps did not consider conduction parameters, and was specified constant cycle length at each point irrespective of its neighbors to show difference in DF map extraction between *N*-FFT and ZP-FFT).

Animal Studies

All animal studies conformed to local and federal guidelines with an approval by Institutional Animal Care and Use Committee, Virginia Commonwealth University.

Optical action potential maps were recorded from isolated rabbit hearts (n=6) during ventricular fibrillation using fluorescence dye (Di-4-ANNEPS, Molecular Probes, Inc., Eugene, OR) and a high speed (100 X 100 pixels, 256 fps) CCD camera (CA-D1-0256T-STDL, DALSA, Ontario, Canada). DF for each pixel of the optical map was

extracted for 1-sec segments resulting in DF maps. DF of individual electrograms and whole DF maps were compared between *N*-FFT and ZP-FFT. Select points (n=118) distributed randomly in the anterior epicardium were selected from the optical maps and cycle lengths (CL) were extracted. The inverse of mean CL was compared with DF obtained using two methods, ZP-FFT and *N*-FFT.

All simulations and data analyses were performed using custom written programs in Matlab, Mathworks® Inc.

Results

Single spectrum peak: When using *N*-FFT, DF detection was perfectly accurate only when the *true* DF fell on one of the samples of the spectrum, i.e. when the true DF was 0, 1/N, 2/N … etc. However, when the true DF was between two discrete frequency samples, *N*-FFT could not accurately extract the DF while ZP-FFT could detect those more accurately. As seen in Figure 1 panel a, the DF was correctly detected using *N*-FFT as 6 Hz since the DF was exactly on one of the sampled frequency. On the other hand, when the actual DF was 6.5 Hz, (Figure 1 panel b) the detected DF using *N*-FFT was 0.5 Hz away from the true DF. So small differences in frequency were not noticeable when *N*-FFT was used to detect DF.

Multiple spectrum peaks: At first glance, it appeared that the detection error was bound by the resolution in *N*-FFT. When the spectrum had multiple peaks, which were spaced far apart from each other in frequencies but with comparable amplitudes, in some cases *N*-FFT detected the wrong peak leading to a large error. This error of DF detection is illustrated in Figure 2. When multiple close lying peaks were present in the signal (as is the case in most real signals), the accuracy of DF detection using ZP-FFT decreased, nevertheless was still better when compared to *N*-FFT.

Maximum precision of ZP-FFT: In a single frequency signal, the error in DF detection for *N*-FFT was up to one-half of the frequency resolution all along the spectrum as shown in Figure 3 due to minimal sampling of the spectrum. In ZP-FFT method, the maximum error occurs when the DF lies near the edge of the spectrum (near DC or near Nyquist frequency) and drops to negligible values when moved slightly away from the edge of the spectrum. Throughout the spectrum, the error in DF detection using ZP-

FFT is lower than the error using *N*-FFT (Figure 3). The mean error in peak detection throughout the spectrum for a single frequency, 1-second signal using *N*-FFT is 0.25 Hz and is 0.022 Hz for ZP-FFT.

Dominant Frequency versus Cycle Length: DF maps are used to study the distribution of rate of excitation in the heart. Inverse of DF reveals the dominant cycle length (CL) during the period. Since the signal is nonstationary during fibrillation, the rate or CL is not constant during the whole period. Hence DF is accepted as a predictor of the *dominant* CL or the *dominant* rate of excitation. Figure 4 shows that ZP-FFT has better correlation ($r^2_{ZP-FFT} = 0.9879$ for ZP-FFT vs. $r^2_{N-FFT} = 0.9292$ for *N*-FFT) with inverse mean CL than *N*-FFT in all types of arrhythmias for randomly selected points (118 points from 6 hearts) on the epicardium.

DF maps: When a DF map is constructed, a possible limitation of *N*-FFT DF detection is that small changes in frequency across epicardial spaces are not detected. Figure 5 (panel a) illustrates the deficiency of *N*-FFT in detecting small changes. High precision DF (HPDF) maps were generated using ZP-FFT as shown in panel b. Several differences could be seen between the two images. Uniform DF values were observed within a DF domain when *N*-FFT was used. This was replaced by a gradual change in frequency in that region in HPDF maps. Some distinct boundaries with stark frequency changes also faded into gradients. Simple ratios between adjacent domains that were observed in *N*-FFT were not always seen when in HPDF maps.

Simulation of DF maps: To validate results, DF map of simulated sine wave map is shown in Figure 6, Again, *N*-FFT could not detect changes smaller than the frequency resolution, but ZP-FFT could detect and express a DF gradient faithfully.

Discussion

Summary of Results

ZP-FFT could detect DF more precisely when there is a single dominant frequency. Even when multiple peaks with comparable amplitudes are present, DF detection using ZP-FFT was more accurate than with *N*-FFT. DF obtained using ZP-FFT correlated with inverse of mean CL better than DF obtained using *N*-FFT. Though CL is not constant during the time segment, DF extracted using *N*-FFT shows quantization-like errors and hence have poorer correlation with CL.

DF maps obtained using *N*-FFT did not show subtle changes in DF values and hence gradient patterns on DF map were unobserved previously, until ZP-FFT method was used. DF maps obtained using *N*-FFT showed several discrete DF domains with uniform DF values within each domain. Boundaries separating domains with large difference in DF values (differences greater than the FFT resolution in cases) have been previously observed (Skanes, Mandapati, Berenfeld, Davidenko, & Jalife 1998;Zaitsev, Berenfeld, Mironov, Jalife, & Pertsov 2000) using *N*-FFT. This and the simple ratio between the two DF values across the boundary have been ingeniously used to explain Wenckebach-like conduction pattern across the boundaries (Samie, Berenfeld, Anumonwo, Mironov, Udassi, Beaumont, Taffet, Pertsov, & Jalife 2001;Zaitsev, Berenfeld, Mironov, Jalife, & Pertsov 2000). Closer look at DF maps show that boundaries did not always demarcate domains with large DF value differences. In some cases, boundaries divided domains with DF difference that was small (equal to the FFT resolution) and in other cases, there was no distinct boundary between two regions of different DF values (Figure 1 in (Samie, Berenfeld, Anumonwo, Mironov,

Udassi, Beaumont, Taffet, Pertsov, & Jalife 2001). Conduction pattern across such areas have not been understood or documented.

When *N*-FFT was used, small changes in DF values within a domain and across domains went unnoticed. When ZP-FFT was used, boundaries separating small DF differences faded in to gradients. Sharp boundaries with large difference in DF values across the boundaries still persisted. We are investigating the mechanism of wave-break at this region with DF gradients. Wenckebach-like conduction used to explain discrete DF domain boundaries, is not a possible mechanism for these DF gradients. The new pattern of DF distribution between DF domains as gradients might throw light in understanding conduction patterns during fibrillation.

Resolution and precision in Fourier methods

The frequency *resolution* of the spectrum depends on the length of the signal in the time domain. Zero padding the signal does not add any data to the signal and hence the resolution remains unchanged. Zero padding is an efficient method for interpolating the spectrum. Though the resolution is fixed, *the precision of peak detection is not always bounded by the resolution*. So increasing the number of frequency samples, increases precision considerably, when using short data segment. Precision of DF detection is not unbounded either. When there are multiple frequencies, interactions of those frequencies will influence the accuracy of DF measurement, which restrict arbitrary accuracy in peak detection. When multiple frequencies are present, larger errors are possible in peak detection using *N*-FFT as shown in Figure 2. Zero-padding

has been proved useful in resolving potential ambiguities in peak detection (Kay & Marple 1981).

In DF maps of fibrillatory tissues, ZP-FFT has better accuracy than *N*-FFT as shown in the results. In fact *N*-FFT can produce DF maps which are not truly depictive of the rate excitation due to the restricted number of frequency samples. (Refer Figure 5)

Windowing techniques

Spectral leakage, which is typical when a rectangular window is used, is observed in Figure 1 and 2. The sidelobes observed can be reduced using a careful selection of a tapering window but always at the expense of reduced resolution (Kay & Marple 1981). Though when using a rectangular window, interaction of the side-lobes with the peak will jeopardize accurate DF detection, using other windows decreased resolution significantly with little or no improvement in accuracy of spectral peak detection. Hence for DF measurement, a rectangular window was proven appropriate. However, it is noted that only peak detection was found to be more accurate using ZP-FFT than with *N*-FFT. Other spectral parameters were not extracted and have not been studied.

Significance of current studies in VF research

A new pattern of gradients of distribution of DF maps in fibrillating hearts was observed when ZP-FFT was used. This new gradient pattern went unnoticed when *N*-FFT was used to detect DF.

We are investigating the mechanism of these intriguing DF gradients observed during VF and attempting to link them to functional three-dimensional scroll waves (as seen in VT and VF), in conjunction with dynamic change in epicardial conduction velocity along the conduction path. These gradient patterns are observed only in VF and not in stable VT with an anatomical obstacle (data presented separately), where the conduction velocity remains the same and the filament is stationary and hence has no wavebreaks. We speculate the variations of epicardial conduction velocity as caused by changing orientation of the rotor filament. The slowing conduction velocity of wavefront propagation on one flank of the phase singularity point will accumulate and may eventually cause epicardial wavebreak at the DF gradient zone. We believe that besides Wenckebach-like conduction reported previously (Zaitsev, Berenfeld, Mironov, Jalife, & Pertsov 2000), the cause for gradient DF may suggest a gradient-based wavebreak not reported before. Further study of DF gradients and its implications for VF maintenance is necessary to make any conclusive remarks.

Conclusions

Use of ZP-FFT while extracting dominant frequencies in VF studies resulted in more accurate DF maps. Gradient patterns of frequency distribution not seen while using *N*-FFT can be seen while using ZP-FFT and might have implications in mechanism of VF.

References

1. Berenfeld, O., Mandapati, R., Dixit, S., Skanes, A. C., Chen, J., Mansour, M., & Jalife, J. 2000, "Spatially distributed dominant excitation frequencies reveal hidden organization in atrial fibrillation in the Langendorff-perfused sheep heart", *J.Cardiovasc.Electrophysiol.*, vol. 11, no. 8, pp. 869-879.

2. Berenfeld, O., Zaitsev, A. V., Mironov, S. F., Pertsov, A. M., & Jalife, J. 2002, "Frequency-dependent breakdown of wave propagation into fibrillatory conduction across the pectinate muscle network in the isolated sheep right atrium", *Circ.Res.*, vol. 90, no. 11, pp. 1173-1180.

3. Chen J, Mandapatti R, Berenfeld O, Skanes A C, & Jalife J 2000, "High-frequency periodic sources underlie ventricular fibrillation in the isolated rabbit heart", *Circulation Research*, vol. 86, pp. 86-93.

4. Kay, S. M. & Marple, S. L. Jr. 1981, "Spectrum analysis - a modern perspective", *Proceedings of the IEEE*, vol. 69, no. 11, pp. 1380-1419.

5. Mansour, M., Mandapati, R., Berenfeld, O., Chen, J., Samie, F. H., & Jalife, J. 2001, "Left-to-right gradient of atrial frequencies during acute atrial fibrillation in the isolated sheep heart", *Circulation*, vol. 103, no. 21, pp. 2631-2636.

6. Oppenheim, A. V. & Schafer, R. W. 1975, *Digital Signal Processing* Prentice-Hall, Inc., Englewood Cliffs, New Jersey.

7. Proakis, J. G. & Manolakis, D. G. 1996, *Digital Signal Processing - Principles, algorithms, and applicaiton* Prentice-Hall, Inc., Upper Saddle River, New Jersey 07458.

8. Samie, F. H., Berenfeld, O., Anumonwo, J., Mironov, S. F., Udassi, S., Beaumont, J., Taffet, S., Pertsov, A. M., & Jalife, J. 2001, "Rectification of the background potassium current: a determinant of rotor dynamics in ventricular fibrillation", *Circ.Res.*, vol. 89, no. 12, pp. 1216-1223.

9. Skanes, A. C., Mandapati, R., Berenfeld, O., Davidenko, J. M., & Jalife, J. 1998, "Spatiotemporal periodicity during atrial fibrillation in the isolated sheep heart", *Circulation*, vol. 98, no. 12, pp. 1236-1248.

10. Valderrabano, M., Yang, J., Omichi, C., Kil, J., Lamp, S. T., Qu, Z., Lin, S. F., Karagueuzian, H. S., Garfinkel, A., Chen, P. S., & Weiss, J. N. 2002, "Frequency analysis of ventricular fibrillation in Swine ventricles", *Circ.Res.*, vol. 90, no. 2, pp. 213-222.

11. Zaitsev, A. V., Berenfeld, O., Mironov, S. F., Jalife, J., & Pertsov, A. M. 2000, "Distribution of excitation frequencies on the epicardial and endocardial surfaces of

fibrillating ventricular wall of the sheep heart", *Circulation Research*, vol. 86, no. 4, pp. 408-417.

Figure Legends

Figure 1: Errors on DF detection using sine and simulated action potential waveforms. Typical N-FFT and ZP-FFT for a validation waveform (sine function: frequency = 6 Hz, amplitude = $\pm$1, duration = 1 s, sampling rate = 256 Hz, data length *N* = 256, and plot range = 0-15 Hz) is shown in panel a. The peak was observed at 6 Hz using 256-FFT. The frequency samples are marked in circles. When the frequency of the signal was changed to 6.5 Hz (panel b), the detected peak still remained 6 Hz, the absolute spectrum value was 84.7 (digital value only no unit) at the peak. With 2560-FFT using zero padded sequence, we could detect the true DF at 6.5 Hz (solid line in panel b) with larger spectral value = 128, 51% higher. Similar results could be seen when action potential waveforms were simulated with constant basic cycle length (BCL). When the DF was exactly on one of the frequency samples of 256-FFT, DF was accurately measured (panel c). For a BCL of 154 (6.5 Hz), 256-FFT detected DF at 6 Hz with spectral value near 5000 while the 2560-FFT reveals DF at accurately at 6.5 Hz with a larger spectral value of near 8000 (panel d).

Figure 2: Error in peak detection using N-FFT can be greater than the resolution of the DFT. Sine waveforms with two frequencies (6.5 Hz and 13 Hz) with different amplitude (1 and 0.8 respectively) were summed to produce the waveform shown in panel a. N-FFT detected DF as 13 Hz. Due to frequency domain sampling, though the power of the spectrum at 6.5 Hz was much larger than at 13 Hz, the true peak was overlooked. This caused an error much larger than the frequency resolution. When ZP-FFT was used for DF detection, the peak was detected accurately as 6.5 Hz. Similar phenomenon is shown in panel b with action potential waveforms. The first five CL in the simulated

waveform were 133 ms (corresponding to a DF of 7.5 Hz) and the last three CL were 100 ms (corresponding to a DF of 10 Hz). Though, the power of the spectrum at 7.5 Hz is higher than at 10 Hz, N-FFT detects 10 Hz as the DF. ZP-FFT however, precisely detects 7.5 Hz as the peak.

Figure 3: Error in DF detection for a single frequency signal. Sine waves of frequencies from zero to Nyquist were generated and the error in DF detection is shown against the frequency (Sampling frequency = 64 Hz). While using N-FFT the error between any two frequency sample reaches up to half the frequency resolution (in this case is 1 Hz) even after disregarding errors with multiple peaks. This error is found throughout the spectrum. On the other hand, when ZP-FFT (100 times zero-padded in this case) is used, the error in DF detection is found only towards the edges of the spectrum (due to interaction with negative frequencies) and rapidly drops down to negligible values as we move in to the spectrum. Even at the edges of the spectrum, the error observed using ZP-FFT does not exceed the error observed when N-FFT is used. The mean error over the whole spectrum for N-FFT is 0.25 Hz in this case and is 0.0225 for ZP-FFT. When multiple frequencies are present in the signal, the error using ZP-FFT increases but will always be lower than the error using N-FFT (not shown).

Figure 4: Correlation between dominant frequency and cycle length. DF has been used to identify rate of excitation or cycle length of underlying tissue. Several (n=118) spatially randomly distributed points in the anterior epicardium was selected to compare mean cycle length measurement with DF obtained by the N-FFT and ZP-FFT. DF obtained by ZP-FFT correlated better (r^2 =0.9879) with the mean cycle length than N-FFT (r^2 =0.9292).

Figure 5: Illustration of DF gradient with HPDF map. Panel a: DF map of the anterior heart using *N*-FFT. Simple ratios can be found between adjacent domains. Panel b: HPDF map of the same data using ZP-FFT to give 10 times more frequency samples with striated bands of DF on left ventricular free wall. The same is not seen in Panel a primarily due to inadequate precision (1 Hz). c and d, enlarged view to show details of the banded structure of DF gradients. A smooth gradient of DF values (0.1 Hz per band and continuous in 6.9 - 8.1 Hz) can be seen in panel d. The scale of gradient in d is limited only by the 0.1 Hz frequency precision. Uniform DF values in each domain seen in *N*-FFT is no longer seen when ZP-FFT is used. (LV = Left Ventricle).

Figure 6: DF of a simulated map of sine waves of specified frequency, Panel a shows the actual distribution of DF for the simulated sine wave signals. Panel b is the DF map obtained using N-FFT with no gradients and sharp boundaries. When ZP-FFT was used to obtain HPDF maps, the domain boundary and the gradients were observed and accurately presented the actual DF values.

Figures

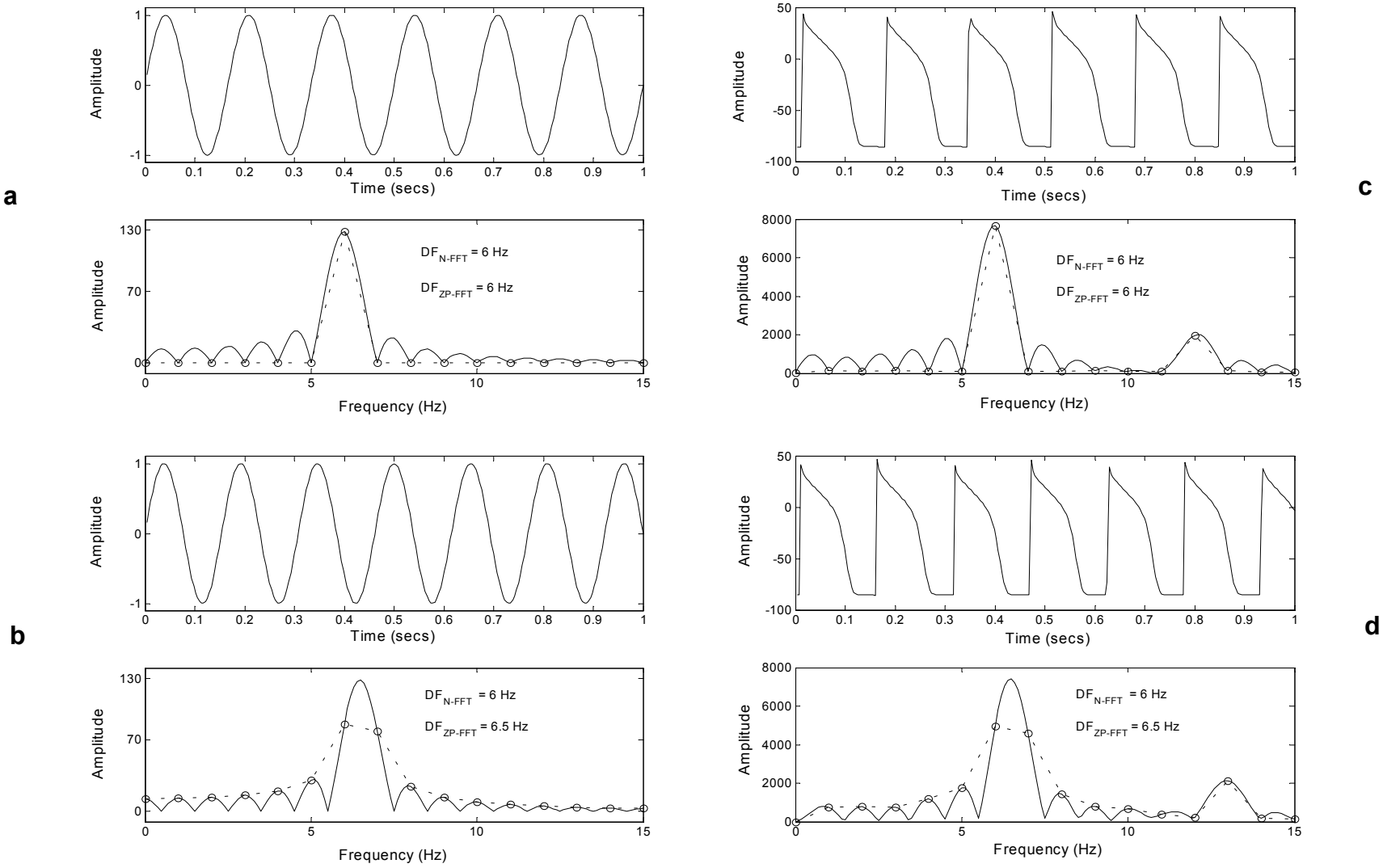

Figure 1

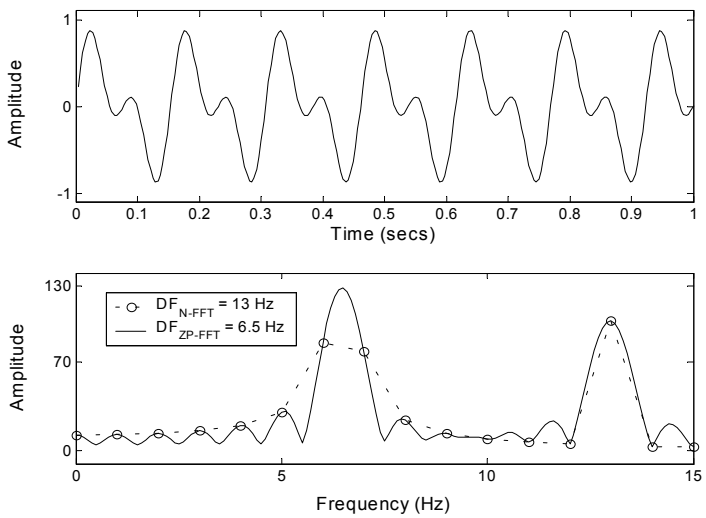
Amplitude
Time (secs)
Amplitude
Frequency (Hz)
DF N-FFT = 13 Hz
DF ZP-FFT = 6.5 Hz

a

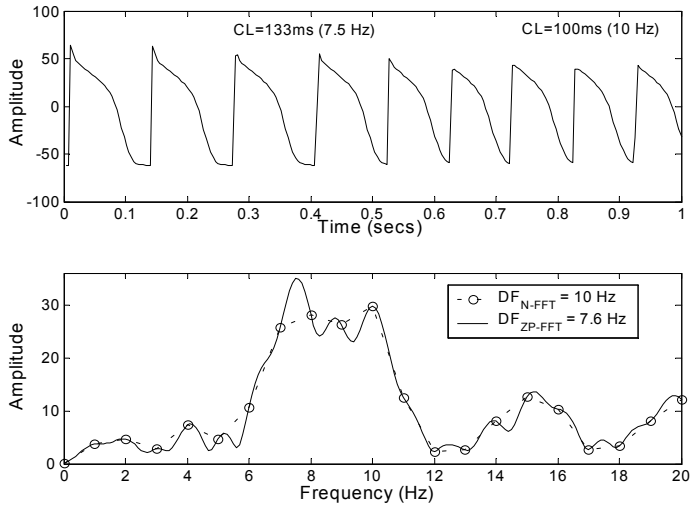
CL=133ms (7.5 Hz)
CL=100ms (10 Hz)
Amplitude
Time (secs)
Amplitude
Frequency (Hz)
DF N-FFT = 10 Hz
DF ZP-FFT = 7.6 Hz

b

Figure 2

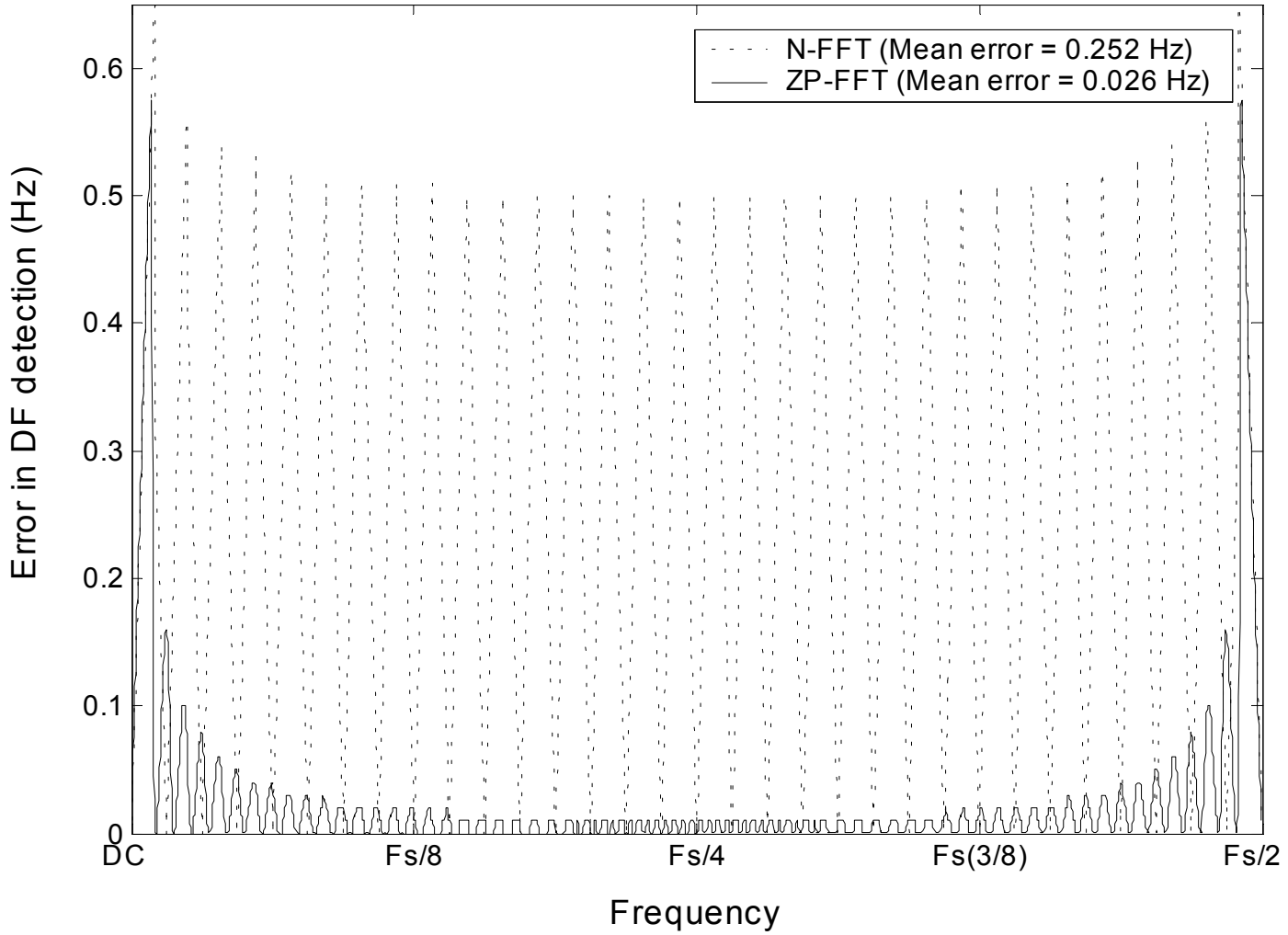
N-FFT (Mean error = 0.252 Hz)
ZP-FFT (Mean error = 0.026 Hz)
Error in DF detection (Hz)
0
0.1
0.2
0.3
0.4
0.5
0.6
DC
Fs/8
Fs/4
Fs(3/8)
Fs/2
Frequency

Figure 3

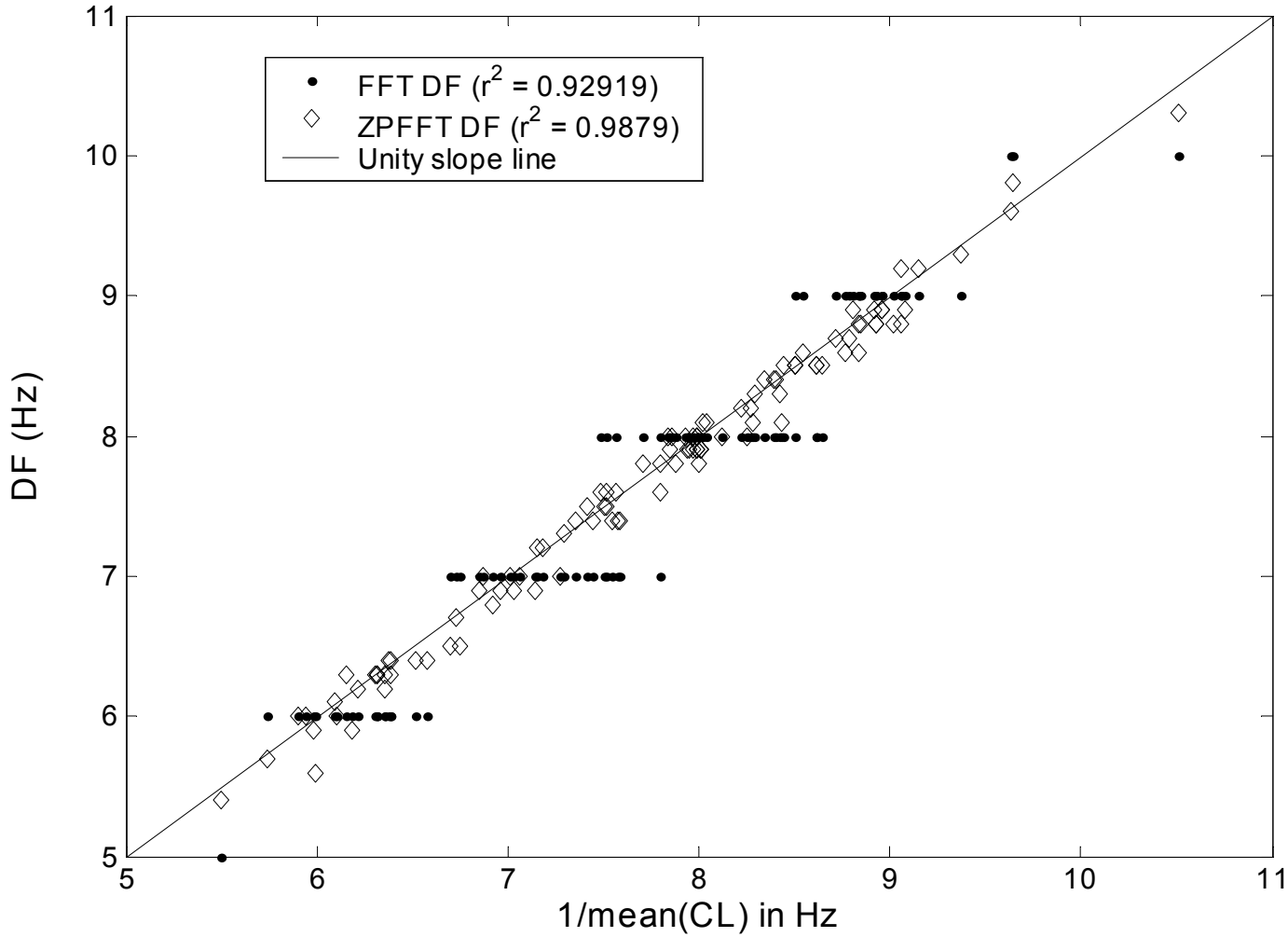
FFT DF (r^2 = 0.92919)
ZPFFT DF (r^2 = 0.9879)
Unity slope line
DF (Hz)
1/mean(CL) in Hz
11
10
9
8
7
6
5
5
6
7
8
9
10
11

Figure 4

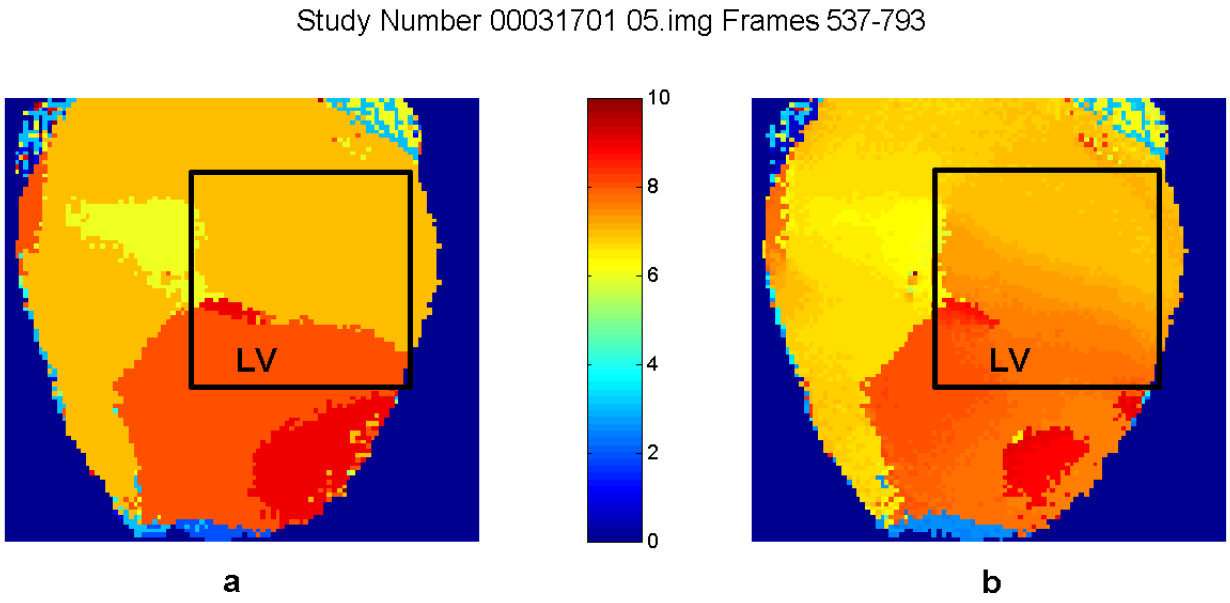
Study Number 00031701 05.img Frames 537-793
LV
10
8
6
4
2
0
LV
a
b

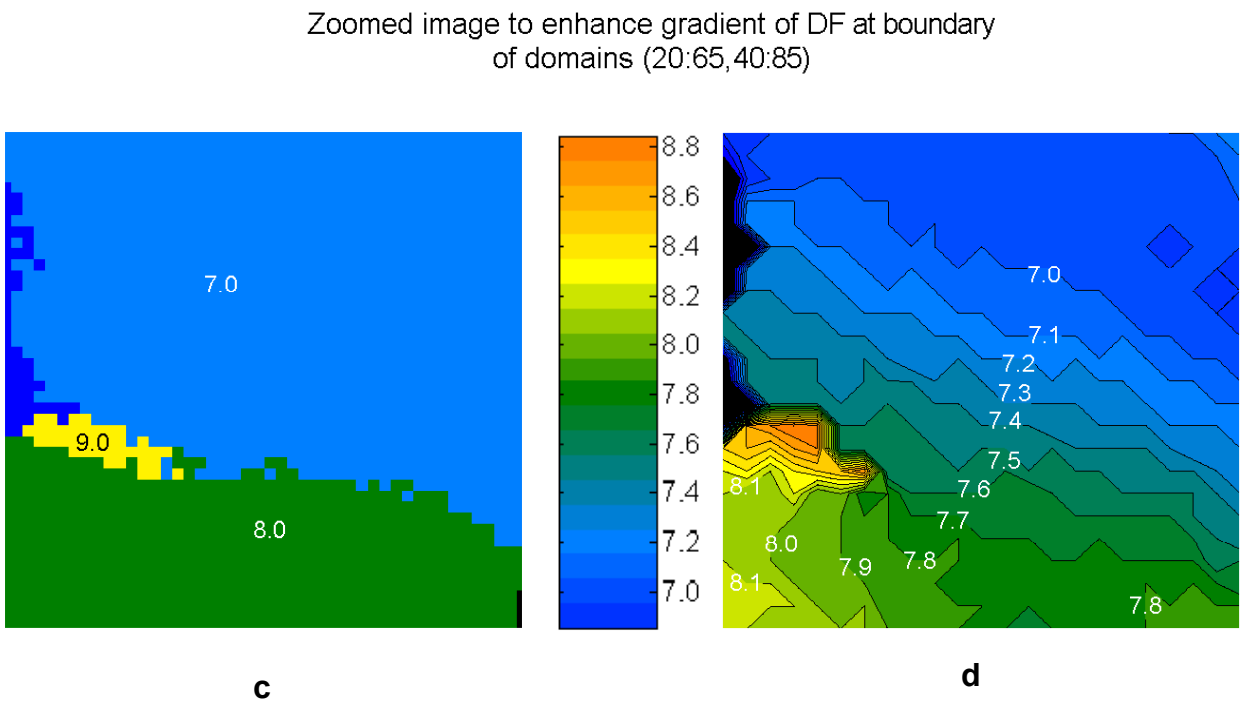
Zoomed image to enhance gradient of DF at boundary
of domains (20:65,40:85)
7.0
9.0
8.0
8.8
8.6
8.4
8.2
8.0
7.8
7.6
7.4
7.2
7.0
7.0
7.1
7.2
7.3
7.4
7.5
7.6
7.7
7.8
7.9
8.0
8.1
8.1
7.8
c
d

Figure 5

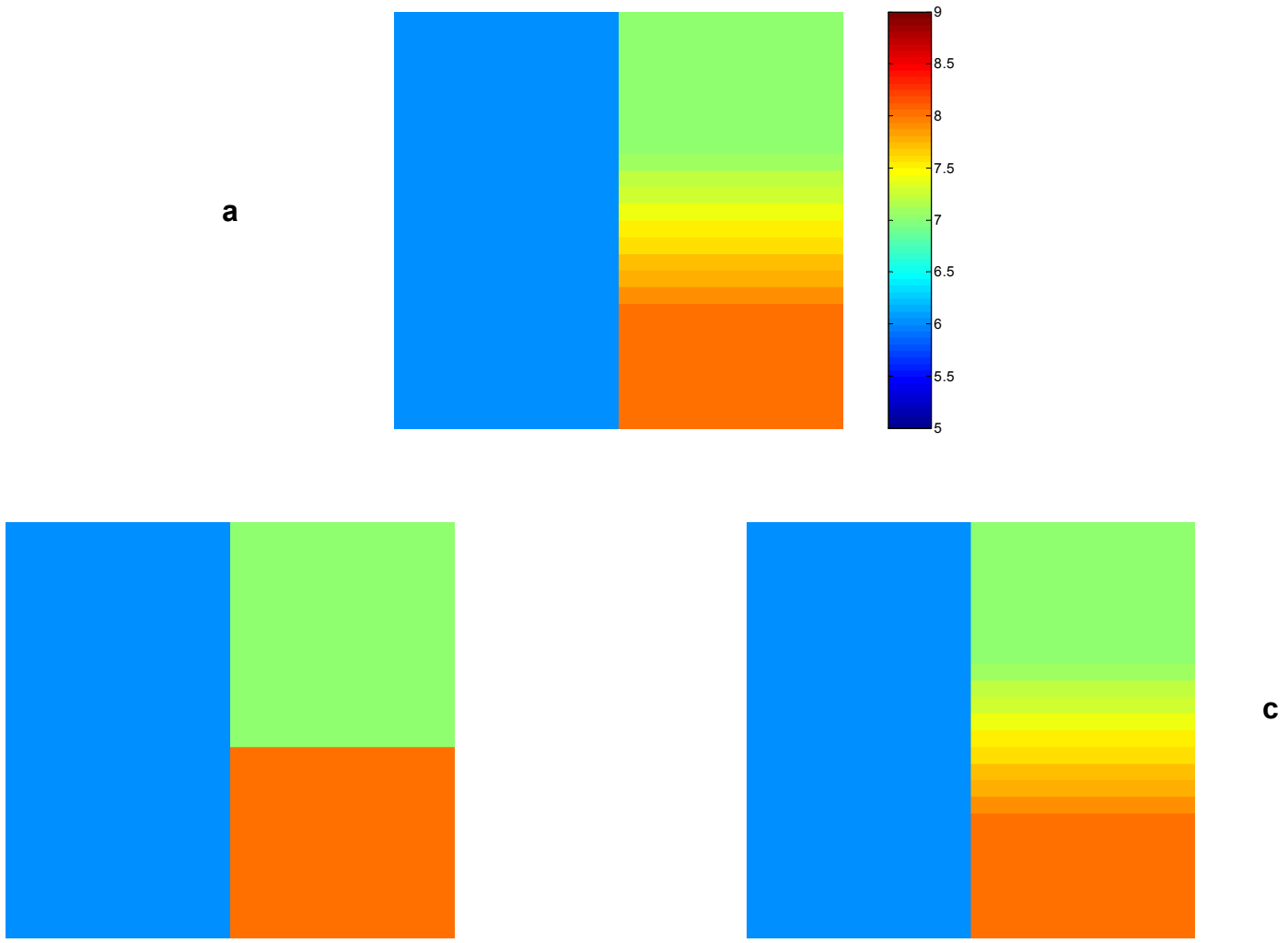

Figure 6